J|A|C|S
ARTICLES
Published on Web 08/02/2006

# Dynamic Nuclear Polarization of Amyloidogenic Peptide Nanocrystals: GNNQQNY, a Core Segment of the Yeast Prion Protein Sup35p

Patrick C. A. van der Wel, Kan-Nian Hu, Józef Lewandowski, and Robert G. Griffin*

*Contribution from the Francis Bitter Magnet Laboratory and Department of Chemistry, Massachusetts Institute of Technology, Cambridge, Massachusetts 02139*

Received April 17, 2006; E-mail: rgg@mit.edu

***Abstract:*** Dynamic nuclear polarization (DNP) permits a $\sim 10^2-10^3$ enhancement of the nuclear spin polarization and therefore increases sensitivity in nuclear magnetic resonance (NMR) experiments. Here, we demonstrate the efficient transfer of DNP-enhanced $^1$H polarization from an aqueous, radical-containing solvent matrix into peptide crystals via $^1$H$-^1$H spin diffusion across the matrix−crystal interface. The samples consist of nanocrystals of the amyloid-forming peptide GNNQQNY$_{7-13}$, derived from the yeast prion protein Sup35p, dispersed in a glycerol−water matrix containing a biradical polarizing agent, TOTAPOL. These crystals have an average width of 100−200 nm, and their known crystal structure suggests that the size of the biradical precludes its penetration into the crystal lattice; therefore, intimate contact of the molecules in the nanocrystal core with the polarizing agent is unlikely. This is supported by the observed differences between the time-dependent growth of the enhanced polarization in the solvent versus the nanocrystals. Nevertheless, DNP-enhanced magic-angle spinning (MAS) spectra recorded at 5 T and 90 K exhibit an average signal enhancement $\epsilon \approx 120$. This is slightly lower than the DNP enhancement of the solvent mixture surrounding the crystals ($\epsilon \approx 160$), and we show that it is consistent with spin diffusion across the solvent−matrix interface. In particular, we correlate the expected DNP enhancement to several properties of the sample, such as crystal size, the nuclear $T_1$, and the average $^1$H$-^1$H spin diffusion constant. The enhanced $^1$H polarization was subsequently transferred to $^{13}$C and $^{15}$N via cross-polarization, and allowed rapid acquisition of two-dimensional $^{13}$C$-^{13}$C correlation data.

## Introduction

In dynamic nuclear polarization (DNP) experiments, the large polarization of electron spins is transferred to the nuclear spins, enhancing the signal intensities by $\sim 10^2-10^3$ for subsequent nuclear magnetic resonance (NMR) spectroscopy,[1−4] an approach that has been demonstrated in several solid-state NMR applications.[5−13] More specifically, the recent development of high-field DNP spectrometers, equipped with gyrotron microwave sources[14,15] and cryogenic magic-angle spinning (MAS) probes,[10,16] have demonstrated promising results for studies of membrane proteins and other biological systems.[9,11,16] In addition, development of biradical polarizing agents[17,18] has significantly improved the enhancement factors of the nuclear polarization in DNP experiments and has concurrently attenuated the residual paramagnetic broadening.

In several previous DNP experiments the nitroxide polarizing agent, 4-amino-TEMPO (4-amino-2,2,6,6-tetramethylpiperidine-1-oxyl) (4AT), was in intimate contact with the solute to be polarized. However, experiments on many macromolecular assemblies require that we consider the possibility that the paramagnet is excluded from close contact with the solute, and thus the question arises if DNP experiments will be applicable to this type of system. In particular, will bulky biradical polarizing agents such as TOTAPOL, consisting of two TEMPO

(1) Overhauser, A. W. *Phys. Rev.* **1953**, *92*, 411−415.
(2) Carver, T. R.; Slichter, C. P. *Phys. Rev.* **1953**, *92*, 212−213.
(3) Carver, T. R.; Slichter, C. P. *Phys. Rev.* **1956**, *102*, 975−980.
(4) Abragam, A.; Goldman, M. *Nuclear Magnetism: Order and Disorder*; Claredon Press: Oxford, 1982.
(5) Wind, R. A.; Duijvestijn, M. J.; Vanderlugt, C.; Manenschijn, A.; Vriend, J. *Prog. Nucl. Magn. Reson. Spectrosc.* **1985**, *17*, 33−67.
(6) Singel, D. J.; Seidel, H.; Kendrick, R. D.; Yannoni, C. S. *J. Magn. Reson.* **1989**, *81*, 145−161.
(7) Afeworki, M.; McKay, R. A.; Schaefer, J. *Macromolecules* **1992**, *25*, 4084−4091.
(8) Afeworki, M.; Vega, S.; Schaefer, J. *Macromolecules* **1992**, *25*, 4100−4105.
(9) Rosay, M.; Zeri, A.-C.; Astrof, N. S.; Opella, S. J.; Herzfeld, J.; Griffin, R. G. *J. Am. Chem. Soc.* **2001**, *123*, 1010−1011.
(10) Rosay, M.; Weiss, V.; Kreischer, K. E.; Temkim, R. J.; Griffin, R. G. *J. Am. Chem. Soc.* **2002**, *124*, 3214−3215.
(11) Rosay, M.; Lansing, J. C.; Haddad, K. C.; Bachovchin, W. W.; Herzfeld, J.; Temkin, R. J.; Griffin, R. G. *J. Am. Chem. Soc.* **2003**, *125*, 13626−13627.
(12) Bajaj, V. S.; Mak, M.; Hornstein, M. K.; Belenky, M.; Herzfeld, J.; Temkin, R. J.; Griffin, R. G. *Biophys. J.* **2005**, *88*, A203.
(13) Mak, M. L.; Bajaj, V. S.; Hornstein, M. K.; Belenky, M.; Temkin, R. J.; Griffin, R. G.; Herzfeld, J. *Biophys. J.* **2005**, *88*, A506.
(14) Hornstein, M. K.; Bajaj, V. S.; Griffin, R. G.; Kreischer, K. E.; Mastovsky, I.; Shapiro, M. A.; Sirigiri, J. R.; Temkin, R. J. *IEEE Trans. Electron Devices* **2005**, *52*, 798−807.
(15) Joye, C. D.; Griffin, R. G.; Hornstein, M. K.; Hu, K.-N.; Kreischer, K. E.; Rosay, M.; Shapiro, M. A.; Sirigiri, J. R.; Temkin, R. J.; Woskov, P. P. *IEEE Trans. Plasma Sci.* **2006**, *34*(3), 518−523.
(16) Bajaj, V. S.; Farrar, C. T.; Hornstein, M. K.; Mastovsky, I.; Vieregg, J.; Bryant, J.; Elena, B.; Kreischer, K. E.; Temkin, R. J.; Griffin, R. G. *J. Magn. Reson.* **2003**, *160*, 85−90.
(17) Hu, K.-N.; Yu, H.-H.; Swager, T. M.; Griffin, R. G. *J. Am. Chem. Soc.* **2004**, *126*, 10844−10845.
(18) Song, C.; Hu, K.-N.; Joo, C.-G.; Swager, T. M.; Griffin, R. G. *J. Am. Chem. Soc.* **2006**. In press.


**10.1021/ja0626685 CCC: $33.50** 

moieties tethered by a three-carbon chain (4-oxy-TEMPO-4-amino-TEMPO-2-propanol), be useful in polarizing for example virus particles, membrane proteins, amyloid fibrils, and peptide and protein nanocrystals? In these cases the sample domains are potentially macroscopically separated from solvent domains containing the polarizing agents. This question was initially addressed by Schaefer et al. when they attempted to transfer enhanced nuclear polarization across a polymer interface[7,19] with the result that they observed no significant enhancements correlated to internuclear spin diffusion. This may partly be ascribed to the fact that the DNP process was based on the solid effect polarizing mechanism using BDPA radicals, which is known to have an inherently low efficiency. In addition, the short nuclear $T_1$ of the polymer material observed at room temperature may have limited the extent of the spin diffusion. Subsequently, Rosay, et al.[9] successfully demonstrated the homogeneous distribution of enhanced polarization in experiments that compared the size of the $^{31}$P and $^{15}$N signal enhancements from the DNA on the inside and the $^{15}$N-labeled coat protein on the outside of bacteriophage, which is ~6.5 nm in diameter. In these experiments, which were performed at ~20 K and employed the more efficient cross-effect DNP polarization mechanism, the $^{31}$P and $^{15}$N signal enhancements were identical, suggesting that spin diffusion distributed the polarization uniformly throughout the solute—the bacteriophage particle. However, the polarizing agent employed was 4AT, and it could have diffused into the phage particles. Further, the phage particles are much smaller than most of the macromolecular assemblies mentioned above (6.5 nm diameter as opposed to >100 nm). We therefore decided to address this question again with studies of another system, nanocrystals of the amyloidogenic peptide GNNQQNY$_{7-13}$ and the improved, but bulky, biradical polarizing agent, TOTAPOL.[18]

GNNQQNY is an excellent system to use in the investigations presented here. The peptide corresponds to the residues 7−13 of the prion-forming protein Sup35p[20,21] found in yeast, and the protein is seen as a model system for an important class of amyloid-related diseases characterized by a preponderance of Gln and Asn residues in the prion-forming protein domains. The GNNQQNY$_{7-13}$ peptide itself resembles the short Gln- and Asn-rich repeats found throughout the Sup35p N-terminal domain and constitutes one of the shortest segments shown to form prion-like fibril aggregates.[22] Upon dissolution in water it also forms nanocrystals on a short time scale with a width varying from 20 nm to 1 $\mu$m,[22,23] and a structure of these species was recently determined with microcrystal X-ray diffraction.[24] Once formed, these crystals, as many amyloid fibrils, resist dissolution, and it is therefore easy to disperse them in cryoprotectants and polarizing agents for DNP experiments. Thus, GNNQQNY$_{7-13}$ is an excellent system to test the applicability of the DNP technique to amyloid peptides, proteins, and other macromolecular assemblies.

Figure 1 is an illustration of the crystal lattice[24] and shows the presence of (a) a water channel with a width of ~0.7 nm, together with (b) a space-filling models of the lattice and a potential average conformation of TOTAPOL, which has limited flexibility in its short linker. An examination of this figure suggests that it is unlikely that the bulky biradical will diffuse into the channel and that the peptide molecules inside the crystallites are in intimate contact with the paramagnetic center. Nevertheless, we observe a substantial enhancement in the nuclear spin polarization ($\epsilon \approx 120$) as opposed to the full enhancement ($\epsilon \approx 160$) observed from the solvent (vide infra). This observation is explained quantitatively by considering the size of the crystals, the nuclear $T_1$, the $^1$H−$^1$H spin diffusion constants, and the initial polarization enhancement of the solvent. In addition, we demonstrate that the enhanced $^1$H polarization can be readily transferred to $^{13}$C and $^{15}$N in the peptide and multidimensional spectra acquired with reduced acquisition periods. Thus, DNP experiments could evolve into vital components of the toolkit used to determine structures of amyloid peptides and proteins as macroscopic nanocrystals and fibrils.

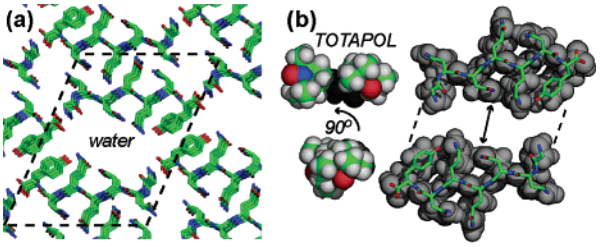


***Figure 1.*** (a) Illustration of the crystal lattice of the GNNQQNY X-ray structure,[24] where the dashed lines delineate two monomers surrounding the largest opening in the lattice, containing a network of hydrogen-bonded water molecules. (b) Space-filling models of the GNNQQNY monomers, the spacing between them (~0.7 nm maximum width), together with two views of an approximate space-filling model of the TOTAPOL biradical showing its size relative to the water opening. The plane of the figure is perpendicular to the longest dimension of the crystallites.

## Theory

We begin with a brief discussion of the processes involved in the application of DNP to insulating solids, involving bulk nuclei doped with dilute concentrations of paramagnets. The DNP process involves transfer of spin polarization from electrons to nuclei, which can occur through at least three different mechanisms, the solid effect (SE),[4] the cross effect (CE),[25−31] and thermal mixing (TM).[5,32] The relative importance of these mechanisms is determined by the relationship between the homogeneous EPR line width ($\delta$) and the nuclear Larmor frequency ($\omega_n$). When the EPR line width is smaller than the nuclear Larmor frequency ($\delta < \omega_n$) only the SE is possible, while the CE and TM are operative when $\delta > \omega_n$. The spin dynamics associated with the SE, CE, and TM involve single, pairwise, and multiple electron spins, respectively. While an

(19) Afeworki, M.; Schaefer, J. *Macromolecules* **1992**, *25*, 4092−4096.
(20) Liebman, S. W.; Derkatch, I. L. *J. Biol. Chem.* **1999**, *274*, 1181−4.
(21) Krishnan, R.; Lindquist, S. L. *Nature* **2005**, *435*, 765−72.
(22) Balbirnie, M.; Grothe, R.; Eisenberg, D. S. *Proc. Natl. Acad. Sci. U.S.A.* **2001**, *98*, 2375−80.
(23) Diaz-Avalos, R.; Long, C.; Fontano, E.; Balbirnie, M.; Grothe, R.; Eisenberg, D.; Caspar, D. L.; Eisenberg, D. S. *J. Mol. Biol.* **2003**, *330*, 1165−75.
(24) Nelson, R.; Sawaya, M. R.; Balbirnie, M.; Madsen, A. O.; Riekel, C.; Grothe, R.; Eisenberg, D. *Nature* **2005**, *435*, 773−8.
(25) Kessenikh, A. V.; Lushchikov, V. I.; Manenkov, A. A.; Taran, Y. V. *Sov. Phys. Solid State (Engl. Trans.)* **1963**, *5*, 321−329.
(26) Kessenikh, A. V.; Manenkov, A. A.; Pyatnitskii, G. I. *Sov. Phys. Solid State (Engl. Trans.)* **1964**, *6*, 641−643.
(27) Hwang, C. F.; Hill, D. A. *Phys. Rev. Lett.* **1967**, *18*, 110−112.
(28) Hwang, C. F.; Hill, D. A. *Phys. Rev. Lett.* **1967**, *19*, 1011−1014.
(29) Wollan, D. S. *Phys. Rev. B: Condens. Mater. Phys.* **1976**, *13*, 3671−3685.
(30) Wollan, D. S. *Phys. Rev. B*: *Condens. Mater. Phys.***1976**, *13*, 3686−3696.
(31) Atsarkin, V. A. *Sov. Phys. USP* **1978**, *21*, 725−744.
(32) Goldman, M. *Spin Temperature and Nuclear Magnetic Resonance in Solids*; Clarendon Press: Oxford, 1970.

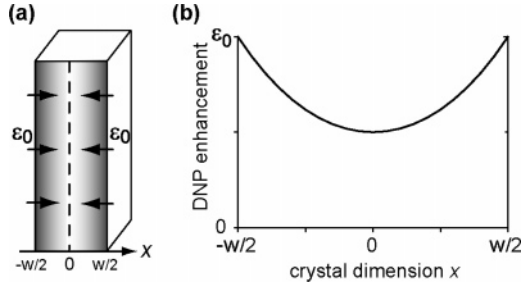


***Figure 2.*** (a) Model for an individual peptide crystallite, showing polarization transfer into the core along the narrowest crystal dimension *x*. (b) Predicted enhanced polarization profile along the dimension *x* of the nanocrystal.

increase in the applied external magnetic field tends to reduce the efficiency of the polarization, the extent of this reduction is dependent on the type of polarization mechanism involved. In the case of the CE and TM, the impact of higher magnetic fields on the polarization transfer efficiency can be compensated by optimizing of the EPR spectral parameters, for example the electron−electron dipole interaction and the EPR frequency separation of the paramagnetic species,[17] for the desired field strength.

The resulting locally enhanced nuclear polarization is distributed to the bulk nuclei via $^1$H nuclear spin diffusion. In a homogeneous sample, the efficiency of this process depends on the density and, possibly, on orientations of nuclear spins. However, the presence of a diffusion barrier,[33,34] for instance resulting from the proximity of a paramagnetic center or two domains characterized by large differences in nuclear spin characteristics, can reduce the efficiency of spin diffusion. The nuclear spin diffusion barrier near a paramagnetic species arises from a strong electron−nuclear dipolar field at the nucleus that isolates the surrounding nuclei in terms of resonance frequency. Similarly, a diffusion barrier can be caused by gaps in resonance frequency between two domains that have different magnetic susceptibilities in response to the external magnetic field.[35−37] This might be a concern for dehydrated nanocrystals embedded in a frozen aqueous solvent matrix. Note that the latter boundary is less intrusive when the domain size is smaller (e.g., in nanometer range).

For simplicity of our discussion, we assume the bulk solvent nuclear spins surrounding the crystals are uniformly polarized with an enhancement factor $\epsilon_0$. The magnitude of this factor is characteristic of the bulk solvent/radical composition and the experimental and instrumental details.[17,18] In our analysis we assume that penetration of enhanced nuclear polarization into a nanocrystal is dominated by uniform nuclear spin diffusion along the smallest dimension of the crystal. This pseudo-one-dimensional (1D) spin diffusion depends on the width of the smallest crystal dimension, the nuclear $T_1$, and the nuclear spin diffusion constant, $D$, of the nanocrystal.

To illustrate our description of the polarization transfer into uniformly sized crystals, we show the model depicted in Figure 2a. A steady-state enhanced polarization of the glass matrix results from microwave irradiation and diffuses into the nanocrystals through the crystal surface. Within the crystal, the enhanced polarization, $\epsilon_0$, diffuses into the core, following a process that is assumed to be dominated by 1D nuclear spin diffusion along the crystal $x$ axis[24] and described by Fick's law:[19,38]

$$\frac{\partial P}{\partial t} = D\frac{\partial^2 P}{\partial x^2} - \frac{P}{T_{1n}} \tag{1}$$

where $P(x,t)$ is the polarization, after subtraction of the Boltzmann polarization, at a time $t$ and a distance $x$ from the center of the crystal; $D$ is the diffusion constant, and $T_{1n}$ is nuclear spin−lattice relaxation time. In the steady-state $\partial P/\partial t = 0$, and we obtain

$$D\frac{\partial^2 P}{\partial x^2} = \frac{P}{T_{1n}} \tag{2}$$

If we assume that the nuclei in the glassy solvent maxtrix have reached a steady-state and that their enhanced polarization is evenly distributed, then we have the boundary condition for the surfaces of the crystals:

$$P\left(\frac{w}{2}\right) = P\left(-\frac{w}{2}\right) = \epsilon_0 P_0 \tag{3}$$

where $w$ is the crystal width along the $x$ axis, $\epsilon_0$ is the steady-state enhancement factor for the solvent nuclear polarization, and $P_0$ is the nuclear Boltzmann polarization at thermal equilibrium. As illustrated in Figure 2b, the solution to eq 2 in the region $-w/2 \le x \le w/2$ with the boundary condition in eq 3 is

$$P(x) = \epsilon_0 P_0 \cosh^{-1}\left(\frac{w}{2\sqrt{DT_{1n}}}\right)\cosh\left(\frac{x}{\sqrt{DT_{1n}}}\right) \tag{4}$$

Experimentally one observes the average polarization across the whole crystal ($-w/2 \le x \le w/2$), as given by

$$\frac{1}{w}\int_{-w/2}^{w/2} P(x)\mathrm{d}x = \frac{2\sqrt{DT_{1n}}}{w}\epsilon_0 P_0 \tanh\left(\frac{w}{2\sqrt{DT_{1n}}}\right) \tag{5}$$

which dictates that the measured enhancement factor $\epsilon$ of the crystals is

$$\epsilon = \epsilon_0 \frac{2\sqrt{DT_{1n}}}{w}\tanh\left(\frac{w}{2\sqrt{DT_{1n}}}\right) \tag{6}$$

The spin diffusion constant $D$ in a proton-rich solid can be estimated as $D = \lambda^2\pi B_L$, where $B_L$ is the average dipolar interaction at a characteristic $^1$H−$^1$H distance $\lambda$. At room temperature, the average dipolar interaction depends on molecular dynamics affecting the proton coordinates.[19] These dynamics are mostly quenched at cryogenic temperatures, except for the three-fold hopping of methyl groups. Nonetheless, the application of sample rotation in solid-state MAS/NMR to the frozen sample can significantly modulate the dipolar interaction. Once the $^1$H−$^1$H dipolar coupling constant $\omega_d$ is smaller than

(33) Blumberg, W. E. *Phys. Rev.* **1960**, *119*, 79−84.
(34) Furman, G. B.; Goren, S. D. *J. Phys.: Condens. Matter* **2002**, *14*, 873−881.
(35) Hurlimann, M. D. *J. Magn. Reson.* **1998**, *131*, 232−240.
(36) Sen, P. N.; Axelrod, S. *J. Appl. Phys.* **1999**, *86*, 4548−4554.
(37) Vasenkov, S.; Galvosas, P.; Geier, O.; Nestle, N.; Stallmach, F.; Karger, J. *J. Magn. Reson.* **2001**, *149*, 228−233.
(38) Lowe, I. J.; Tse, D. *Phys. Rev.* **1968**, *166*, 279−291.

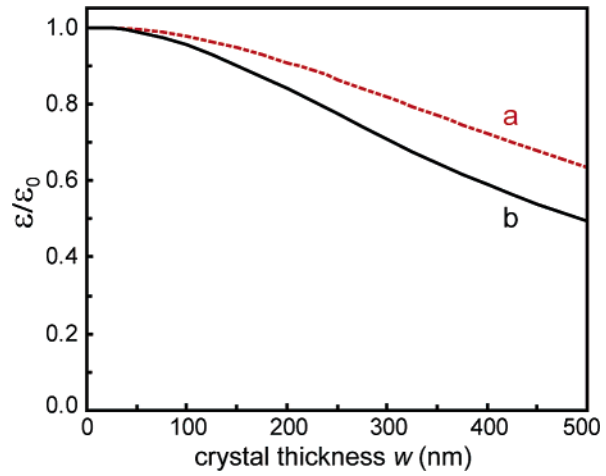


***Figure 3.*** Theoretical enhancement $\epsilon$, compared to the homogeneous enhancement $\epsilon_0$ in the glassy matrix, of proton polarization in a nanocrystal of width $w$. The calculation uses a proton $T_{1n} = 17$ s, and the calculated values of the diffusion constant (a) $D = 2 \times 10^5$ and (b) $1 \times 10^5$ Å$^2$/s.

the spinning frequency $\omega_r$, average Hamiltonian theory[39] suggests $B_L \propto (\omega_d)^2/\omega_r$. Based on the published crystal structure [24] combined with computational modeling, the $^1$H−$^1$H distances along the two shortest crystal axes range from 2.0 to 3.2 Å for a continuous trajectory throughout the crystal, resulting in $\omega_d/2\pi$ of 15−3.5 kHz. Notice that the magic-angle spinning at $\omega_r/2\pi \approx 5$ kHz has little effect for these magnitudes of the $^1$H−$^1$H dipolar interaction. In other words, the corresponding spin diffusion constant $D$ should approximate $(1 \times 10^5)$ to $(2 \times 10^5)$ Å$^2$/s. Typical experimental values that were previously obtained for a variety of organic polymers ranged from 2 to $8 \times 10^4$ Å$^2$/s,[40−43] but these are likely to reflect the presence of more molecular dynamics than are present in our system, related to higher temperatures and more mobile moieties including methyl groups. Using the estimated diffusion coefficients $D$ and measured $T_{1n}$ (∼17 s, vide infra) with eq 6, we can predict the theoretical enhancement factor of the $^1$H polarization in GNNQQNY$_{7-13}$ as a function of crystal size, as illustrated in Figure 3. These predicted DNP enhancements in nanocrystals will be compared to experimental results from DNP measurements and TEM observations.

## 3. Experimental Section

**Peptide Nanocrystal Samples.** The peptide GNNQQNY was synthesized using solid-phase synthesis methods in both a natural abundance form, and a segmentally, isotopically labeled form [U-$^{13}$C,$^{15}$N-GNNQ]QNY by CS Bio Co. (Menlo Park, CA). A mixture of 20% labeled and 80% unlabeled material was mixed and then crystallized as follows. A solution of 10 mg/mL in deionized water was filtered through a 0.2 $\mu$m filter to remove residual particles and then crystallized for at least 24 h at 4 °C. This protocol yields homogeneous monoclinic nanocrystals.

**DNP Experiments.** The DNP samples were prepared by washing the fully crystallized sample several times with 80/20 $D_2O/H_2O$, then mixed with 60/30/10 glycerol-$d_8$/$D_2O$/$H_2O$, containing 10 mM of biradical polarizing agent. The extent of deuteration in the solvent system is optimized for optimal channeling of the DNP proton-polarization to the sample material of interest, while maintaining the proton−proton spin diffusion necessary for distribution of the polarization throughout the sample. The deuterated solvents were obtained from Cambridge Isotope Laboratories (Andover, MA). The biradical TOTAPOL, composed of two TEMPO moieties tethered by a five-atom linker, was synthesized as described elsewhere.[18] The resulting heterogeneous mixture, containing a total of ∼20 mg of peptide, was center-packed into a 4-mm sapphire MAS rotor. A similarly prepared, undiluted sample consisting of 100% [U-$^{13}$C,$^{15}$N-GNNQ]QNY crystals hydrated in deionized water was used as a reference sample.

All DNP-enhanced CP/MAS experiments were performed in a 5 T superconducting magnet ($^1$H frequency of 212 MHz) with a superconducting sweep coil capable of changing the magnetic field by ±750 G. A custom-designed probe was used to perform triple resonance experiments (two rf frequencies ($^1$H, $^{13}$C) and a waveguide provided for irradiation of the 4-mm sample with microwaves) during MAS (∼4−6 kHz) at ∼90 K.[10] High-power, 139.66-GHz microwaves were obtained from a gyrotron (∼10 W output power) delivering ∼1.5 W to the sample. Since there is not a resonant microwave structure in the probe, the quality factor is low ($Q \approx 1$) for the microwave radiation. The $Q$ of the rf circuit is not perturbed by the microwave waveguide. The pulse sequence[17] begins with saturation of $^1$H polarization by a series of 90° pulses and delays (10 ms) followed by a period of polarization recovery (1−75 s). Application of microwaves during the recovery period leads to a buildup of enhanced $^1$H polarization that is subsequently transferred to the $^{13}$C or $^{15}$N spins through ramped cross-polarization (CP) (spin-lock for 1.2 ms with a constant 30 kHz $^1$H field and a ramped 26−30 kHz $^{13}$C field). The resulting $^{13}$C and $^{15}$N CP signals were detected using ∼70 kHz TPPM $^1$H decoupling.[44] The two-dimensional (2D) $^{13}$C−$^{13}$C correlation experiment was performed using DNP enhancement after 5 s of microwave irradiation and involved $^{13}$C−$^{13}$C mixing with 6 ms of $^1$H-driven spin diffusion assisted by a $^1$H radio frequency field matching the n=1 rotary resonance condition (known as Dipolar Assisted Rotational Resonance (DARR),[45] or Radio Frequency Field Assisted Diffusion (RAD)[46] mixing). It was executed in the absence of the saturating proton pulses with the following experimental details: 5 s recycle delay, 56 $t_1$ points of four scans each, resulting in approximately 20 min of acquisition time. The data were processed using NMRPipe.[47]

**Transmission Electron Microscopy.** A Philips EM410 electron microscope was used to examine the peptide crystals by transmission electron microscopy (TEM) before and after the DNP measurements. TEM micrographs were obtained after negative staining with aqueous uranyl acetate. The dimensions of numerous peptide nanocrystals were measured by comparison to calibration micrographs of reference grid samples (Electron Microscope Sciences, Hatfield PA).

## 4. Results and Discussion

**4.1. Enhanced NMR Signal Intensities of Peptide Nanocrystals.** One-dimensional CP/MAS NMR data recorded for the 20% labeled peptide nanocrystal sample in the absence of DNP yielded relatively poor signal-to-noise spectra. The measurements were repeated in the presence of microwave irradiation, which resulted in a dramatic increase in the signal intensity, as illustrated in Figure 4. The signal-to-noise without microwave irradiation was insufficient to observe well-resolved spectral lines for the (20%) isotopically labeled $^{13}$C. However, in the

(39) Maricq, M. M.; Waugh, J. S. *J. Chem. Phys.* **1979**, *70*, 3300−3316.
(40) Chen, Q.; Schmidt-Rohr, K. *Solid State Nucl. Magn. Reson.* **2006**, *29*, 142−152.
(41) Cheung, T.; Gerstein, B. *J. Appl. Phys.* **1981**, *52*, 5517.
(42) Clauss, J.; Schmidt-Rohr, K.; Spiess, H. W. *Acta Polym.* **1993**, *44*, 1−17.
(43) Jia, X.; Wolak, J.; Wang, X.; White, J. L. *Macromolecules* **2003**, *36*, 712−718.
(44) Bennett, A. E.; Rienstra, C. M.; Auger, M.; Lakshmi, K. V.; Griffin, R. G. *J. Chem. Phys.* **1995**, *103*, 6951−6958.
(45) Takegoshi, K.; Nakamura, S.; Terao, T. *Chem. Phys. Lett.* **2001**, *344*, 631−637.
(46) Morcombe, C. R.; Gaponenko, V.; Byrd, R. A.; Zilm, K. W. *J. Am. Chem. Soc.* **2004**, *126*, 7196−7197.
(47) Delaglio, F.; Grzesiek, S.; Vuister, G. W.; Pfeifer, J.; Bax, A. *J. Biomol. NMR* **1995**, *6*, 277−293.

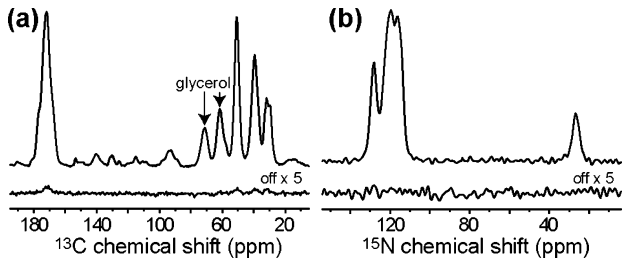


***Figure 4.*** DNP-enhanced $^{13}C$ (a) and $^{15}N$ (b) CP/MAS spectra of [20% U-$^{13}C$,$^{15}N$-GNNQ]QNY in $d_8$-glycerol/$D_2O$/$H_2O$ (60/30/10) with 10 mM TOTAPOL biradical at 90 K and 5 T, with (top trace) and without (bottom trace) DNP. The microwave power was 1.5 W, and irradiation time was 75 s for both spectra.

presence of microwaves even the natural abundance $^{13}C$ signals could be seen (from the unlabeled residues in the segmentally labeled peptide and the glycerol in the frozen solvent matrix). The same enhancement effect is observed for the $^{15}N$ spectrum, where the signals were undetectable in the absence of DNP, but are rather intense with DNP enhancement. The maximum observed enhancement was quantified to be $\epsilon \approx 120 \pm 10$ after 75 s of microwave irradiation, relative to the $^{13}C$ spectrum without DNP. Note that the NMR signals of the solute (e.g., the glycerol carbons) in the glass matrix are also strongly enhanced, with an estimated enhancement $\epsilon_0 \approx 160$, based on previous measurements. The intensity of the $^{15}N$ signals without microwave irradiation was too weak to allow an accurate measurement of the enhancement, but its enhancement should be similar to that measured for the peptide $^{13}C$'s since both are determined by the polarization enhancement of the $^1H$ spins.

While the signal intensity in the absence of DNP was too low for a 2D NMR experiment to be practical, the observed DNP enhancement stimulated us to perform a 2D experiment to evaluate the applicability of DNP to this and other amyloid samples. This involves a 2D $^{13}C-^{13}C$ homonuclear correlation experiment with 6-ms spin diffusion mixing. The results are shown in Figure 5, and the combined acquisition time of the entire experiment required approximately 20 min. This of course compares extremely favorably with the anticipated acquisition time in the absence of DNP. Note that one can discern several signals from the natural abundance Tyr side chain, further highlighting the high enhancement factor resulting from the microwave irradiation.

The assignments of the cross-peaks in the spectrum are indicated in the figure and were based on experiments performed at higher fields to be described in a separate publication. As mentioned, we observe the natural abundance glycerol peaks on the diagonal, which are broadened because of the amorphous nature of the frozen glass matrix and the proximity of the biradical species. The presence of a substantial radical concentration in a solution is known to cause significant broadening in any co-dissolved solute. Especially when using high concentrations of less efficient polarizing agents, this is also seen in DNP experiments on frozen solutions. In contrast, the crystalline nature of the sample shields the molecules on the interior of the crystals from both the glassy solvent and the direct interaction with the radicals (except for narrow regions near the crystal surface), resulting in peptide peaks that are narrower than the glycerol signals. However, the peptide signals are significantly broader than those observed in our assignment experiments mentioned above, where the spectra were recorded

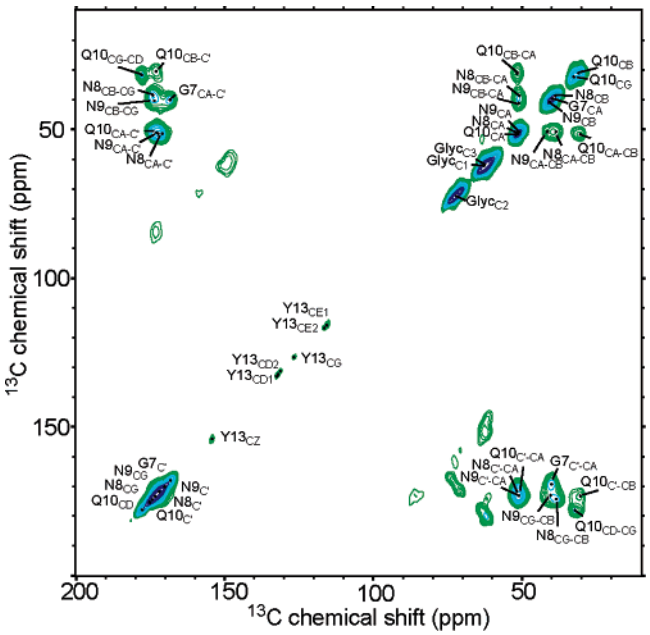


***Figure 5.*** DNP-enhanced $^{13}C-^{13}C$ DARR/RAD correlation spectrum of [20% U-$^{13}C$,$^{15}N$-GNNQ]QNY nanocrystals. Indicated assignments are based on previous assignment data, and unmarked cross-peaks represent spinning sidebands and experimental artifacts.

on a 500 MHz instrument. To evaluate whether any broadening is due to the experimental DNP conditions and examine whether it could be indicative of the radical having direct access to a significant portion of the peptide, we performed a number of tests. In room-temperature spectra comparing the glycerol- and TOTAPOL-containing DNP sample to a non-DNP reference sample (lacking glycerol and radicals) we observe the same line width for both samples, which also matches the line widths at low temperature. This fact, plus the observation that the spectra of the reference sample are narrow at high fields, suggest that the additional line width is not due to the glass formation or interaction with the radicals, but rather arises from $n = 0$ rotational resonance effects.[39,48] These effects are important when the shift separation is comparable to the dipolar coupling and the spinning frequency is low as was the case in these experiments. For a more sensitive test for the penetration of TOTAPOL biradicals into the crystals, we performed room-temperature measurements at higher field (700 MHz $^1H$ frequency) and faster spinning (15 kHz MAS) comparing GNNQQNY nanocrystals before and after the addition of the biradical (see Supporting Information). The line widths in these data are significantly smaller (approximately $100 \pm 2$ Hz for the various labeled $^{13}C$ carbons and as low as $35 \pm 2$ Hz for the N-terminal glycine-$^{15}N$) and should be sensitive to broadening by nearby radicals. Even at a concentration of 50 mM TOTAPOL, 5 times the amount used in the DNP experiments, no broadening of the carbon and nitrogen line widths was observed, confirming the absence of radicals from the inside of the crystals.

The recycle delay for the acquisition of the 2D spectrum was significantly shorter than that required for the development of the full DNP-enhanced polarization of the $^1H$'s in the crystals and reflects a compromise between a large signal enhancement

(48) Levitt, M. H.; Raleigh, D. P.; Creuzet, F.; Griffin, R. G. *J. Chem. Phys.* **1990**, *92*, 6347−6364.

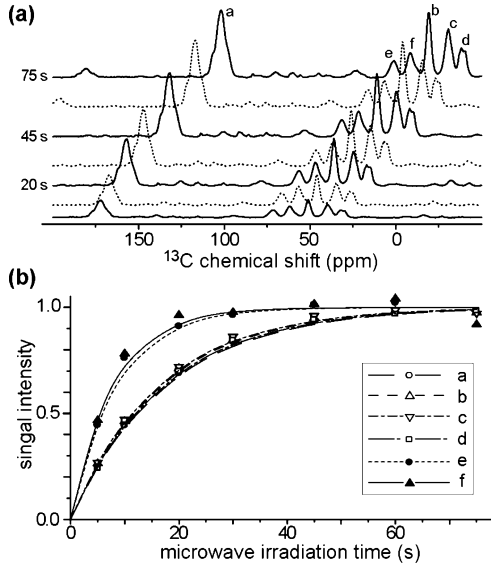


***Figure 6.*** Time-dependent growth of the enhancement polarization. (a) Illustration of the 1D $^{13}C$ spectra as a function of microwave irradiation time, after 5, 10, 20, 30, 45, 60, and 75 s of microwave irradiation. The chemical shift axes are offset for visual clarity. (b) The intensity of the spectral lines normalized to maximum intensity of each signal. Lines indicate calculated fits using growth time constants of 16−17 s for crystal signals (a−d), and 7−8 s for glycerol peaks e and f.

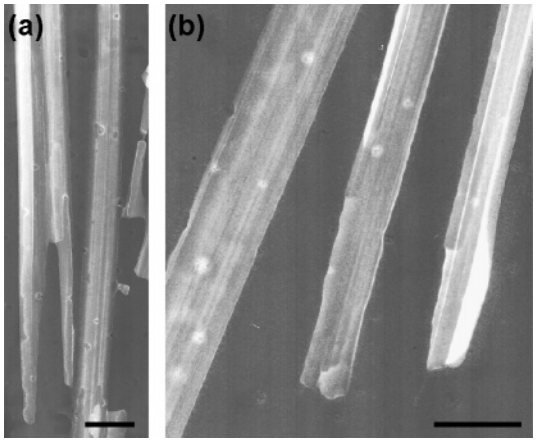


***Figure 7.*** Transmission electron micrographs of GNNQQNY nanocrystallites at an approximate magnification of (a) 55,000 and (b) 110,000. The black bars indicate 200 nm.

and the phase cycling requirements of the experiment. The result of this choice of recycle delay is that the relative intensities of the glass-embedded glycerol solvent relative to the peptide signals are shifted in favor of the solvent signals, reflecting a difference in the polarization rate between the crystals and the solvent molecules. This difference is further illustrated in a series of 1D experiments, examining the buildup of magnetization as a function of the microwave irradiation time. These experiments were performed according to the procedure described previously,[17] and the resulting $^{13}C$ spectra confirm that the polarization buildup for the glycerol is substantially faster than that for the peptide crystal signals (Figure 6). The time constants for the glycerol signals, ranging from 7 to 8 s, are shorter than those of the nanocrystal signals which range from 15.5 to 17 s. The presence of the biradicals at 10 mM reduces the $^1H$ $T_{1n}$ in the glassy solvent, giving a rapid polarization transfer and shorter time constants for polarization. Since the peptide crystals exclude the TOTAPOL, polarization time constants in the crystals reflect the intrinsic $^1H$ $T_{1n}$, which is relatively long due to the low temperatures and determines the internuclear spin diffusion within the crystals. Note that, in general, relatively long spin−lattice relaxation times are necessary for optimal DNP enhancement. We will now correlate the diffusion constant, $T_{1n}$, and the size of the nanocrystals with the observed enhancement using the Fick's law treatment discussed above.

**4.2. Polarized Portions of Fibril Crystals.** On the basis of the TEM micrographs illustrated in Figure 7, we were able to measure the dimensions of the nanocrystals in the samples used to record the DNP enhanced spectra shown in Figures 4−6. The average width of the crystals approximates 150 nm, with a typical range between 100 and 200 nm. The distribution of crystal sizes in these samples is not entirely uniform, with a few exceptions of significantly thicker or thinner (down to ∼50 nm) width. Narrowing of the crystals tends to occur at their ends. These observations correspond well to previously published TEM data and dimensions of GNNQQNY nanocrystals.[24]

We will now compare these experimental observations to the predicted relative enhancements in Figure 3, obtained using the Fick's law formula in eq 6 together with the estimates of the $D$ and measured values of $T_{1n}$. The central assumption in that calculation that the biradical TOTAPOL does not penetrate the crystals was originally based on the realization that the size of TOTAPOL exceeds the width of the water channel in these crystals (see Figure 1) and was reinforced by the observed reduction of the enhancement inside the crystals. Further experimental data, including the longer peptide $T_{1n}$ compared to that of the solvent and the absence of changes in the line widths in the peptide crystals in the presence or absence of TOTAPOL radicals (see Supporting Information for MAS spectra illustrating this point) indeed show that there is no significant direct interaction between the radical and the bulk of the peptide nanocrystals.

Considering that the polarizing agent is absent from the crystal core, direct polarization of the crystal surface layer alone is unable to explain the observed large crystal signal enhancement. Rather it is due to diffusion into the crystals of the enhanced nuclear polarization $\epsilon_0 P_0$ uniformly present throughout the solvent matrix, and at the surface of the crystals, as described in section 2. There, we estimated the $^1H$ spin diffusion constants as lying in the range $(1 \times 10^5)$ to $(2 \times 10^5)$ Å$^2$/s. On the basis of these assumptions and the measured $T_{1n} \approx 17$ s, we predicted the enhancements to be observed in crystals with various characteristic widths (Figure 3). In our case we observed an average crystal enhancement $\epsilon$ that is ∼0.75 (120/160) of the enhancement $\epsilon_0$ in the bulk solvent matrix. Combined with the crystal dimensions that were observed in our TEM experiments (100−200 nm), this result falls slightly under the curve shown for the lower diffusion constant. Considering the relatively simple nature of the applied model, it is unclear whether very detailed conclusions concerning the exact value of the spin diffusion rate can be drawn on the basis of these results. The lower rate could indicate that the effective diffusion rate is limited by a "bottleneck" across the direction of transfer that is not apparent in the crystal structure, possibly near the crystal−solvent interface. Inhomogeneity and anisotropy in the crystal packing could affect the effective spin diffusion constant.

Furthermore, one could also consider other experimental features such as the distribution of crystal sizes and possible factors affecting the uniformity of the surface polarization and the diffusion pattern.

## 5. Conclusions

We have shown that DNP experiments are applicable to enhancing the $^1$H polarization of peptide nanocrystals of ~100−200 nm width, yielding intense NMR signals and significant reductions in acquisition times. The increased signal intensity opens new possibilities for significantly more complex and informative pulse experiments to be performed on relatively dilute samples. Dilution of the isotopically labeled sample is often essential when intermolecular interactions have to be suppressed, as is the case for small molecules such as the peptides studied here. DNP enhancement would allow a high level of dilution, while maintaining sufficient signal intensity for accurate and sensitive NMR measurements.

One of the limiting aspects of the data shown here is the limited resolution that can be achieved on this relatively low-field prototype equipment. Ongoing experiments on different instrumentation[14,16] in our group have demonstrated the acquisition of higher-resolution DNP spectra.[12,13] We note that the experiments discussed here show little or no sign of additional broadening due to the cooling to 90 K, or the presence of the radicals (even at 5 times increased concentration in the high-field, high-MAS reference experiments). These observations can be attributed to the nature of these crystals, which are very tightly packed and exclude both the TOTAPOL radicals and the amorphously freezing solvent system.

The exclusion of the bulky biradical polarizing agent from the crystal lattice highlights the importance of $^1$H−$^1$H spin diffusion in DNP experiments on heterogeneous samples. We presented a simple calculation based on 1D spin diffusion that explains the observed extent of polarization and correlates it to the observed crystal size. A more detailed evaluation of the exact role of spin diffusion in these experiments, and further quantification, would benefit from further experiments with particles (or crystals) of a carefully controlled size. The theory discussed here (supported by our data) would suggest that nanocrystals with a size up to 1 $\mu$m can be efficiently polarized, opening avenues for further applications of DNP to studies of protein microcrystals. Further experiments with a wider variety of crystalline and fibril compounds should provide further insights into the importance of sample features such as the presence of methyl groups, molecular motion, and crystal packing for spectral features such as low-temperature resolution, nuclear spin diffusion, and the achievable DNP enhancement.

**Acknowledgment.** This research was supported by the National Institutes of Health through Grants EB-002804, EB003151, and EB-002026. Thanks are accorded to Dr. Chan-Gyu Joo for helpful conversations during the course of these experiments.

**Supporting Information Available:** Figure S1 shows the results of high-field (700 MHz $^1$H) line width measurements on the peptide nanocrystals with and without TOTAPOL polarizing agent, confirming the lack of biradical penetration into the crystals. This material is available free of charge via the Internet at http://pubs.acs.org.

JA0626685